


ORIGINAL ARTICLE

Open Access



# The effect of delignification ratio on the PMMA occupation in poplar wood cell wall by the macro and micro comparative study

Haiyang Zhang<sup>1,2,3\*</sup> , Fucheng Xu<sup>1,4</sup>, Linlin Xu<sup>1</sup> and Chaowei Zheng<sup>1</sup>

## Abstract

The polymer/wood functional products may not be true nanocomposites due to the poor permeability of non-polar monomers into the hydrophilic wood cell wall. In this paper, methyl methacrylate (MMA) chosen as the representative non-polar monomer was used to impregnate wood with different lignin removal and then polymerized in situ in delignified wood to obtain polymethyl methacrylate/delignified wood (PMMA/DW). The larger 10 nm mesopores reduction in PMMA/DW-29.9 and the disappearance of the smaller 3 nm mesopores of PMMA/DW-51.7 indicated that the removal of lignin was beneficial for the penetration of MMA in the wood cell wall. When the lignin removal reached between 29.9 and 51.7%, the dimensional stability of PMMA/DW was improved, and it could be speculated that the resin began to enter the wood cell wall at this stage. In addition, the indentation modulus and hardness of the PMMA/DW cell wall were significantly increased when the lignin removal reached 29.9%. This result was consistent with the conclusion of the pore size analysis, which further confirmed that the nanopores of the cell wall were filled with PMMA when the lignin removal was greater than 29.9%. The results of this paper indeed provide a basis for the design of biomass functional nanocomposites.

**Keywords** Wood composite, Cell wall, Permeability, Porosity, Modification

## Introduction

Wood is a renewable and naturally degradable biomass material. It was ubiquitously used in the construction field for its lightweight, high strength, high modulus, and low thermal conductivity. Unlike other building materials such as steel, cement, and plastics, wood has a unique three-dimensional porous structure with cellulose as the

skeleton, lignin, and hemicellulose as filling and cementing substances [1, 2]. Among them, the unique porous structure, microscale, nanoscale hierarchical structure, and pronounced anisotropy give it a series of remarkable characteristics, which provide the possibility for the design of wood-based functional materials [3, 4]. In the past decade, the function of wood has extended to applications beyond construction by optimizing the structure and composition of wood through physical, chemical, or combined modification methods [5, 6]. In recent years, wood-based functional materials have been widely used in many fields, such as the development of high-performance structural materials, energy storage and conversion, environmental remediation, light or thermal management, and so on [7, 8]. A series of products with excellent performance have appeared, such as transparent wood [9–11], conductive wood [12], oil-absorbing wood sponge [13], wood hydrogel [14–16], wood aerogel

\*Correspondence:

Haiyang Zhang  
zhynjfu@njfu.edu.cn

<sup>1</sup> College of Materials Science and Engineering, Nanjing Forestry University, Longpan Road 159#, Nanjing 210037, China

<sup>2</sup> Jiangsu Co-Innovation Center of Efficient Processing and Utilization of Forest Resources, Nanjing Forestry University, Nanjing 210037, China

<sup>3</sup> International Innovation Center for Forest Chemicals and Materials, Nanjing Forestry University, Nanjing 210037, China

<sup>4</sup> Institute of Chemical Industry of Forest Products CAF, Nanjing 210037, China

[17–19], ultra-flexible wood [20, 21], and shape memory wood [22]. The increase in the use of wood materials is driven by a variety of factors, including reducing carbon emissions, increasing energy, and supporting sustainable industrialization. However, the high porosity and specific surface area of wood-based templates usually were required to facilitate efficient penetration of polymer monomers when the functional materials were prepared. To further increase the porosity of the wood-based template, there are currently two main solutions. The first is the called “bottom-up” strategy, which uses mechanical or chemical methods to separate the cellulose fibrils in the wood, and then reassemble the separated fibrils to obtain a wood-based template with high porosity [23–25]. The other is the so-called “top-down” strategy, which uses chemical methods to remove lignin from wood and retain the original wood frame [26, 27]. The high porosity and specific surface area can be obtained by this method [19]. The “top-down” strategy has many advantages compared with the “bottom-up”, the most typical of which is a simple process and reduced energy consumption [27]. In addition, this method retains the original fiber arrangement in the wood. Compared with the non-directional arrangement structure formed by reassembling after fiber separation, the oriented and ordered structure makes the wood-based template have more excellent mechanical properties.

However, the following problems are still being faced in functional materials manufactured by polymer infiltration to delignification templates. First, wood has a strong polarity because it contains a large number of hydroxyl groups. Many polymers used to make wood-based functional materials tend to have low polarity, which makes them poorly compatible with wood, causing most of the polymer monomers to only fill the wood cell lumen and cannot penetrate the cell wall. Without cell wall penetration, it will be difficult to give full play to the functions and mechanical properties of wood-based functional materials leading to the materials prepared therefrom are not true polymer nanocomposites [28, 29]. In addition, lignin is deposited around cellulose microfibrils with a width of 25–30 nm to strengthen the cell wall structure [30]. The removal of lignin will damage the complete structure of wood, resulting in a change of pore structure in wood and a decrease in the elastic modulus and hardness of wood cell walls [31]. The introduction of polymers into the cell wall significantly impacts the physical and mechanical properties of wood-based functional materials.

Methyl methacrylate (MMA) is a common monomer used to make transparent wood based on a delignified template. It has been widely studied because of its refractive index similar to that of cellulose, low price,

and simple polymerization process [32]. However, MMA exhibits poor permeability in wood cell walls because of its low polarity. Previous studies have shown that if MMA monomer impregnates wood in liquid form, the polymer only fills the wood cell lumen and cannot be further dispersed in the cell wall [33]. This will not be able to prepare wood-based nanocomposites, which affects the function of wood-based functional materials and limits the improvement of the physical and mechanical properties of the materials. Li et al. used delignified wood as a template and MMA as a filling monomer to prepare transparent wood [10]. The mechanical results showed that transparent wood has better tensile strength than delignified wood and pure polymethyl methacrylate (PMMA), which suggested that the polymer was successfully dispersed in the cell wall. However, this has not been confirmed and the polymer distribution was unknown. Several researchers have used Raman spectroscopy to analyze the distribution of resin in the wood cell wall, and the characteristic functional group  $-\text{CH}_2$  representing PMMA was discovered. However, the peaks corresponding to  $-\text{CH}_2$  overlapped with certain chemical components of wood, which increased the difficulty of data analysis [34]. In addition, due to the limited resolution of Raman microscopes, this further reduced the accuracy of PMMA distribution characterization in wood cell walls. Recently, Chen et al. verified that PMMA was distributed in the transparent wood cell wall in nanometer size by small-angle neutron scattering (SANS) technology [33]. The results showed that the pattern of SANS of PMMA/wood biocomposite showed a peak, which indicated that PMMA was distributed in the cell wall in a nanoscale, which confirmed its nanocomposite structure. In addition, the cell wall structure remained inflated due to the use of the solvent exchange method. This allowed PMMA to be distributed not only in the cell wall, but also in the area between cellulose elementary fibrils with a few nanometers in size. This was due to the use of the solvent exchange method to make the MMA monomer impregnation process similar to the natural lignification process.

The polymer/wood functional products may not be true nanocomposites due to the poor permeability of non-polar monomers into the hydrophilic wood cell wall. Therefore, a series of problems may arise, such as the function of polymer/wood composites cannot be well realized, in addition, the dimensional stability and mechanical properties of the composites will also be affected. Herein, we obtained wood templates with different lignin removal by adjusting the chemical treatment time. The delignified wood templates were subsequently impregnated with MMA prepolymer under vacuum, and after two-stage curing, polymethyl methacrylate/delignified wood composites (PMMA/DW) with different

lignin removal were obtained. Through cold field emission scanning electron microscope (FE-SEM), attenuated total reflection Fourier infrared spectroscopy (ATR-FTIR), nitrogen adsorption test, volumetric anti-swelling efficiency (ASE), moisture sorption test, dynamic mechanical analysis (DMA) and nanoindentation test, the morphology, permeability, dimensional stability and micromechanical properties of PMMA/DW were explored. Moreover, the effect of lignin removal level on the permeability of MMA in the cell wall was judged. This study provides a strong basis for designing biomass nano-functional composites.

## Experimental

### Materials

Poplar wood (*Populus, L.*) were provided by Suqian Hongwei Wood Industry Co., Ltd. (Suqian, Jiangsu, China). Sodium chlorite ( $\text{NaClO}_2$ , 80 wt %), glacial acetic acid ( $\text{CH}_3\text{COOH}$ , AR, 99.5%), sodium acetate ( $\text{CH}_3\text{COONa}$ , AR, 99%), methyl methacrylate (MMA, CP, molecular weight 100.12, 98%), azobisisobutyronitrile (AIBN, 98%) were purchased from Macleans Biochemical Technology Co., Ltd. (Shanghai, China). The solvents including deionized (DI) water and absolute ethanol were used.

### Delignification process

The poplar (*Populus, L.*) sapwood specimens with 10 mm (longitudinal, L)  $\times$  10 mm (tangential, T)  $\times$  10 mm (radial, R) were selected for the study. Before chemical treatment, all the samples were dried at  $(103 \pm 2)^\circ\text{C}$  for 24 h until reaching a constant mass ( $m_0$ ) after rinsing with DI and ethanol. The dried samples were then extracted with 2 wt%  $\text{NaClO}_2$  and acetate buffer solution (pH 4.6) at  $80^\circ\text{C}$ . The different lignin removal specimens were obtained by adjusting the treatment time for 6, 9, 12, 18, and 24 h. The delignified liquid was replaced every 6 h to keep the modification efficient. Subsequently, the extracted samples were soaked in enough distilled water for 12 h to thoroughly remove the residual chemical reagents. After the rinse, the samples were freeze-dried with a vacuum of 20 Pa at  $-50^\circ\text{C}$  for 15 h. The specimens were then weighed and recorded as  $m_1$  (absolute dry weight) after totally freezing dried. The delignified wood was marked as DW. In addition, for dimensions of 60 mm  $\times$  10 mm  $\times$  2.5 mm samples, delignified for 2, 4, 6, 9, and 12 h, respectively, were used for the DMA test.

### Preparation of PMMA/DW composites

A certain amount of MMA monomer was first weighed and 0.3 wt% AIBN was added. The solution was moved into an Erlenmeyer flask and placed in a water bath at  $75^\circ\text{C}$  for 15 min. Then, the flask was quickly cooled with

ice water to prevent an explosion. The DW was put into an impregnation tank and kept under 5 kPa for 30 min to extract air from the wood. Subsequently, the MMA prepolymer was sucked into the impregnation tank and submerged samples. Then the tank was returned to normal atmospheric pressure and kept for 2 h to let the polymer flow into the samples. Next, the impregnated specimens wrapped in the aluminium foil were kept at  $(75 \pm 2)^\circ\text{C}$  for 4 h after removing the excess monomer and then were heated up to  $(105 \pm 2)^\circ\text{C}$  to fully solidify the prepolymer until the weight was constant. After removal from the oven, the samples were weighed and recorded as  $m_2$  (absolute composite dry weight).

### Characterization methods

The lignin content of the original wood and DW was determined according to GB/T 747–2003 Pulps—determination of acid-insoluble lignin. Firstly, the specimens were extracted by Soxhlet extractor with the benzene–alcohol mixture (volume ratio 2:1) for 6 h. Secondly, they were placed in a 250 ml Erlenmeyer flask after being air-dried and the pre-prepared  $(72 \pm 0.1)\%$  sulphuric acid solution was added with shaking. The process was kept for 2 h at  $20^\circ\text{C}$ . Thirdly, all the contents in the 250-ml Erlenmeyer flask were transferred into a 2000-ml Erlenmeyer flask and the acid concentration was diluted to 3% with distilled water. The insoluble matter was precipitated after being boiled for 4 h. After that, the deposits were filtered and washed with hot distilled water until they showed neutral. Finally, the filter paper and residue were moved into a weighing bottle and dried in an oven at  $(105 \pm 3)^\circ\text{C}$  to a constant weight to measure the acid-insoluble lignin ( $m$ ). The acid-insoluble lignin content  $X$  (%) was calculated according to Eq. 1:

$$X(\%) = \frac{m}{m_1} \times 100\%, \quad (1)$$

where  $m$  is the weight of the completely dried acid-insoluble lignin and  $m_1$  is the weight of the completely dried natural wood and DW.

The oven-dried mass and volume of the specimens were measured to calculate the density and weight percent gain (WPG) using 10 replicates. The WPG was calculated according to Eq. 2:

$$\text{WPG}(\%) = \frac{m_2 - m_1}{m_1} \times 100\%, \quad (2)$$

where  $m_2$  is the oven-dried weight of the composite PMMA/DW and  $m_1$  is the totally dried weight of DW.

The micro-morphology of the original wood, DW, and PMMA/DW was investigated by a cold field emission scanning electron microscope (JSM-7600E, JEOL Ltd.) under an accelerating voltage of 3 kV, and the

cross-sectional surface of the sample was cut using an ESM-150 s slide microtome (Elma, Japan). ATR-FTIR spectra of the samples were recorded on a VERTEX 80 V spectrometer (Bruker, Germany) over the scan range of 400–4000  $\text{cm}^{-1}$ . The surface area and pore size distribution were analyzed by the nitrogen adsorption device (ASAP 2020 HD88, Micromeritics, USA) at 77 K. Before the measurements, samples were out-gassed at 100 °C for 6 h to remove the water vapor. The specific surface area ( $S_{\text{BET}}$ ) was calculated according to the Brunauer–Emmett–Teller method (BET). The pore size distribution was determined by the Barrett–Joyner–Halenda (BJH) method.

The dimensional stability of the natural wood and PMMA/DW were determined according to GB/T1932.2-2009 Method for determination of the swelling of wood. Firstly, the samples were dried at 60 °C until reaching a constant dimension. Then, the samples were placed at a temperature of  $(20 \pm 2)$  °C and a relative humidity of  $(65 \pm 3)\%$  to absorb moisture until dimensionally stable. During the moisture absorption process, the size change along the grain direction was measured every 6 h and the size was considered to be stable when the difference between the two measurement results did not exceed 0.1 mm. Finally, the samples were immersed in distilled water up to the time their size stabilized. The method of checking whether the sample size has been stable was similar to the moisture absorption process except for a 0.01 mm measurement change. The swelling coefficient ( $\alpha$ ) and anti-swelling efficiency (ASE) can be calculated by Eqs. 3–6:

$$\alpha_{65\%} = \frac{V_{65\%} - V_0}{V_0} \times 100\%, \quad (3)$$

$$\alpha_{\text{max}} = \frac{V_{\text{max}} - V_0}{V_0} \times 100\%, \quad (4)$$

$$\text{ASE}_{65\%} = \frac{\alpha_{65\%(\text{C})} - \alpha_{65\%(\text{P})}}{\alpha_{65\%(\text{C})}} \times 100\%, \quad (5)$$

$$\text{ASE}_{\text{max}} = \frac{\alpha_{\text{max}(\text{C})} - \alpha_{\text{max}(\text{P})}}{\alpha_{\text{max}(\text{C})}} \times 100\%. \quad (6)$$

In the formula,  $\alpha_{65\%}$  represents the volumetric swelling coefficient of the sample at 65% RH;  $\alpha_{\text{max}}$  represents the volumetric swelling coefficient of the sample when it is saturated with water.  $V_0$ ,  $V_{65\%}$ , and  $V_{\text{max}}$  are the volume of the sample when it is absolutely dry, absorbs moisture, and absorbs water to dimensional stability, respectively.  $\text{ASE}_{65\%}$  and  $\text{ASE}_{\text{max}}$  are the volumetric anti-swelling efficiency of moisture absorption and water absorption, respectively.  $\alpha_{65\%(\text{C})}$  and  $\alpha_{65\%(\text{P})}$  are

the volumetric swelling coefficient of natural wood and PMMA/DW under moisture absorption, respectively.  $\alpha_{\text{max}(\text{C})}$  and  $\alpha_{\text{max}(\text{P})}$  are the volumetric swelling coefficient of natural wood and PMMA/DW under water absorption, respectively.

The dynamic mechanical analysis (DMA) of the control and PMMA/DW samples were conducted by the Q800 (TA, US) in the double cantilever beam mode. The samples with dimensions 60 mm  $\times$  10 mm  $\times$  2.5 mm (L  $\times$  T  $\times$  R) were scanned over a range of 30 to 250 °C with an increased speed of 3 °C/min and frequency of 2 Hz. The micromechanical properties of wood cell walls were evaluated by nanoindentation (iMicro, Nano Force, US) with 5 mm  $\times$  5 mm  $\times$  5 mm (L  $\times$  T  $\times$  R) samples, the surface of samples was processed by Leica ultracut R-type ultrathin slicer (Leica, Germany). The samples were all placed at 20 °C and 65% relative humidity for 48 h before the test. The maximum load tested was 400  $\mu\text{N}$  and the loading and unloading rates were both 80  $\mu\text{N/s}$ . The load was maintained for 5 s when it reached the maximum. The indentation modulus and hardness of the cell wall were calculated according to the research of Tze et al. [35].

## Results and discussion

### Lignin removal process

Figure 1 shows that the wood color changed with the extension of the delignification duration. It changed from brown to yellow and finally to white with different process times. The reasons for the radical transformation in color are that lignin is the main light-absorbing component in wood and there are many chromophoric groups in lignin structure such as carbonyl groups, carboxyl groups, and alkene conjugated with benzene rings [36, 37]. In addition, there are many auxochrome groups such as phenolic hydroxyl and alcoholic hydroxyl. These chromophoric and auxochromic groups present in the structure of lignin are the main foundation of wood color. Table 1 shows lignin content changes of modified wood and the corresponding lignin removal level. More lignin in the wood cell wall was taken away as the modification time was prolonged. The lignin content was reduced and the structure was destroyed resulting in a color alternation.

### Impregnated properties

Figure 2a is the schematic diagram of the preparation of PMMA/DW and FE-SEM photos of original wood, delignified wood with 97.3% lignin removal (DW-97.3) and PMMA filled 97.3% delignified wood (PMMA/DW-97.3) are shown in Fig. 2b–d, respectively. It could be seen from Fig. 2b that wood fiber cells were mainly composed of empty cell lumens and solid cell walls.

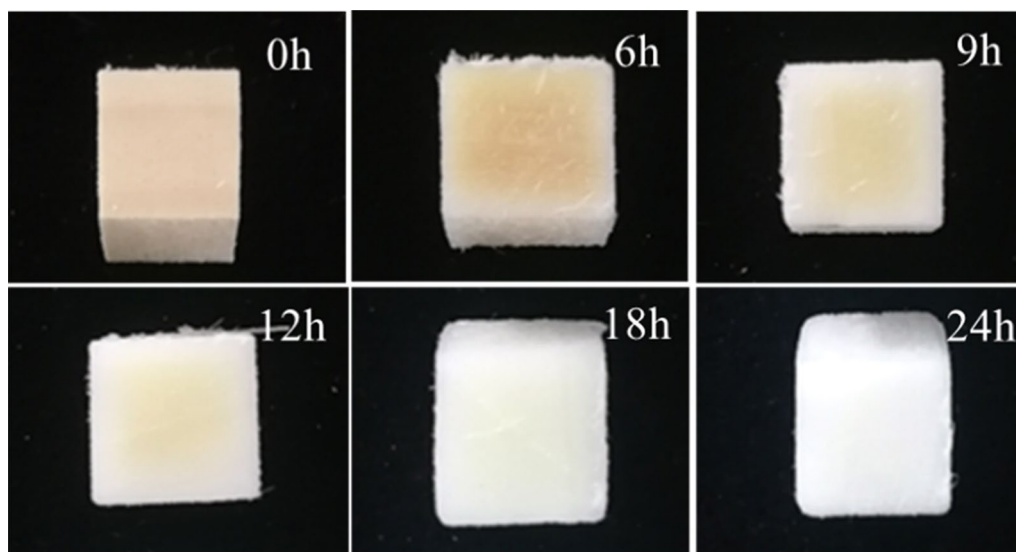


**Fig. 1** The original wood and delignified wood (DW). The numbers in the pictures represent the time spent in delignification

**Table 1** The relationship between lignin removal and treatment time

Time (h)	Lignin content (wt %)	Lignin removal (%)
0	22.8 (0.9)	0
6	18.83 (1.27)	17.4
9	15.98 (2.2)	29.9
12	11.01 (1.76)	51.7
18	6.11 (0.22)	73.2
24	0.62 (0.03)	97.3

Values in parentheses are standard deviations

The cell wall is composed of substantial materials which provide the basis for the density and mechanical properties of wood [38]. The space between adjacent wood fiber cell walls contains the middle lamella and the cell corner, both of which have very high lignin content [39, 40]. It can be observed from Fig. 2c that there were obvious gaps in the intercellular layers between the cell walls and the cell corners after the delignification treatment. In addition, the rough structure of the cross-section of the cell wall could be easily observed with greater magnification. Nano-scale pores appeared on the secondary wall, which was consistent with previous research results about the microstructure of DW [7]. Figure 2d shows that almost all wood cell lumens were filled with PMMA and the pores created by the chemical treatment in the intercellular layer and cell wall corners were also almost fully occupied. Compared with DW-97.3, the cell wall of

PMMA/DW-97.3 become smooth and the nanoscale pores on the secondary wall were also filled. Nevertheless, the degree of filling at the micro- and nano-levels needs to be further explored. In most cases, it is not necessary to remove almost all lignin when designing related functional composite materials that are time and energy-consuming and environmentally unfriendly.

The WPG and density of PMMA/DW are shown in Fig. 3. When the lignin removal level was lower than 29.9%, the WPG of PMMA/DW was 110 wt% with no significant difference among the 0, 17.4, and 29.4% groups. When the removal level reached 51.7%, the WPG increased to 125%, which was significantly higher than the wood with less delignification. After that, WPG still increased with further lignin removal. This was mainly due to the appearance of more void space in the wood cell walls as the lignin was removed, which facilitated the penetration and solidification of plastic in the cell wall. In addition, when the lignin removal percentage attained 51.7%, the density of the composite material increased from the original  $0.47 \text{ g/cm}^3$  to  $0.95 \text{ g/cm}^3$ , an increase of 102%. Subsequently, the density of PMMA/DW went on climbing with more serve delignification. The density of PMMA/DW come up to  $1.15 \text{ g/cm}^3$  when the lignin removal level achieved 97.3%, which was almost the same as the density of pure PMMA [41].

The lignin removed from the original wood was also confirmed by FTIR analysis (Fig. 4). The characteristic bond at 1593, 1505 (lignin aromatic ring C=C stretching vibration) and  $1462 \text{ cm}^{-1}$  (aromatic skeleton vibration) of lignin disappeared gradually after prolonged

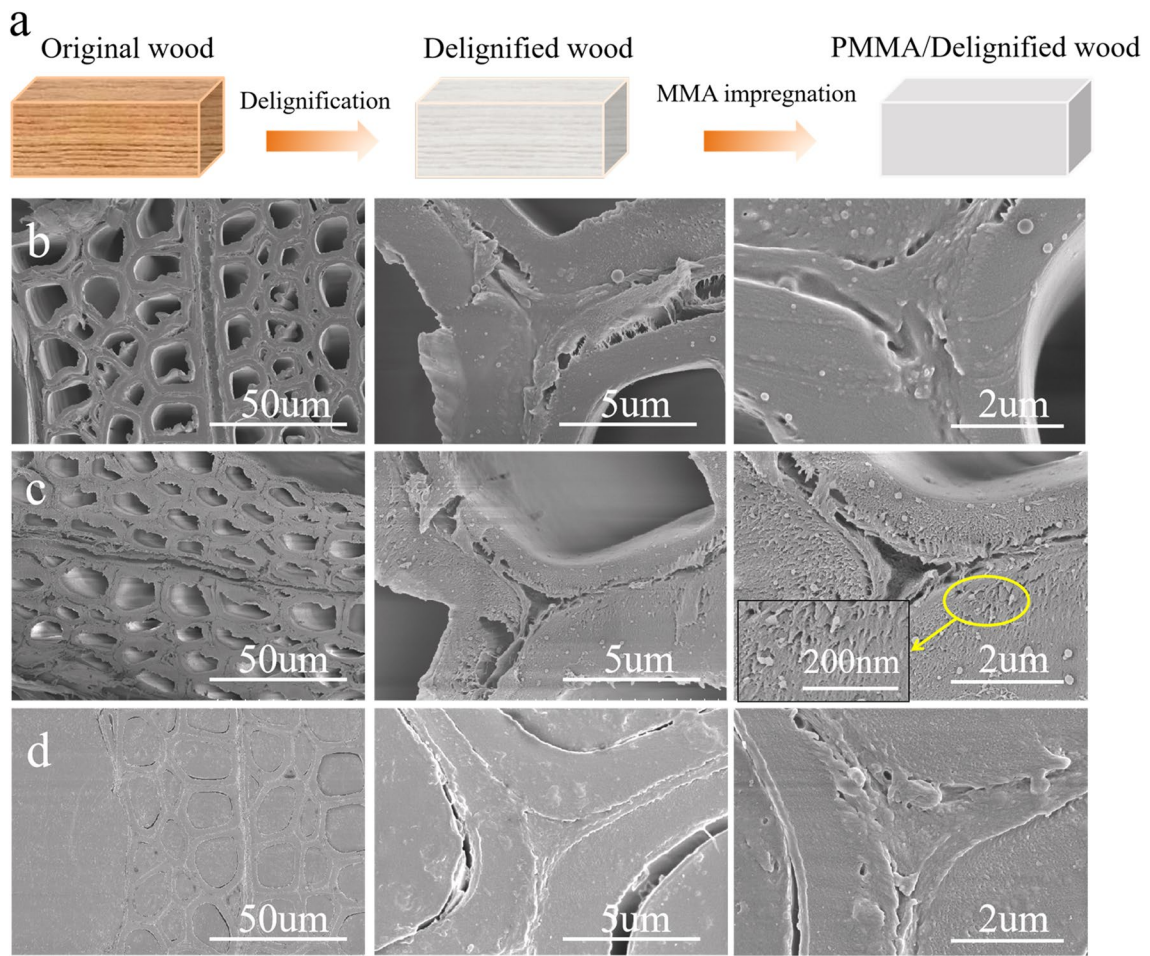


**Fig. 2** The preparation schematic diagram of PMMA/DW (a) and the FE-SEM images of original wood (b), DW-97.3 (c), PMMA/DW-97.3 (d)

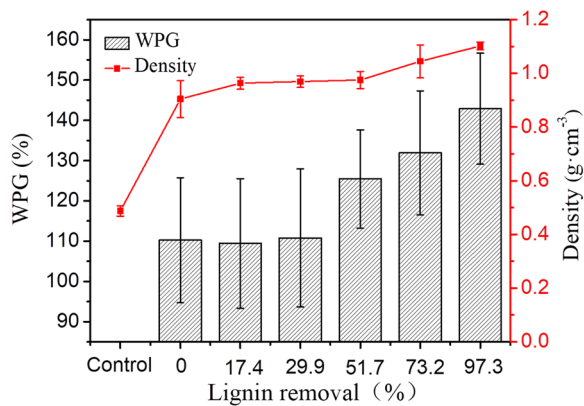


**Fig. 3** The WPG and density of PMMA/DW

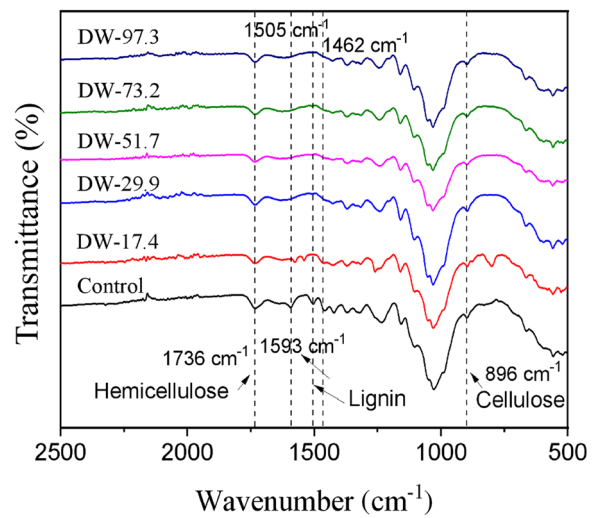


**Fig. 4** FTIR of natural wood and DW

delignification chemical treatment. The characteristic bond of hemicellulose at  $1736\text{ cm}^{-1}$  and cellulose at  $896\text{ cm}^{-1}$  was retained in all samples, confirming the process selectivity for lignin removal.

### Pore characteristics

Nitrogen adsorption was used to analyze the pore size and PMMA distribution in wood cell walls. The nitrogen adsorption and desorption isotherms of original wood, DW, and PMMA/DW are shown in Fig. 5. Obviously, the DW could absorb more nitrogen and the nitrogen adsorption capacity gradually increased with the processing degree upraised (Fig. 5a). After being plastic impregnated and solidified, the adsorption of nitrogen was greatly reduced (Fig. 5b). In addition, hysteresis was obvious in all DW samples while in the polymer-impregnated DW was very limited. Figure 6a shows the pore size distribution in the range of 2–18 nm of natural wood and DW and the accumulative pore volume in the wood cell wall. The peak appeared at about 3 nm in the original wood indicating that there were more mesopores in this diameter range, which was similar to the results of previous research [42]. The number of mesopores around 3 nm increased with delignification, as shown by the increased intensity of the peak there. The heightening in the specific surface area and total pore volume of DW with delignification in Table 2 also confirmed the transformation of the number of mesopores and pore diameters caused by “top-down” delignification. Comparing Fig. 6a and b shows the change in pore size and volume when PMMA

was added. Based on PMMA/DW-0, PMMA/DW-17.4 had an obvious peak at 10 nm and PMMA/DW-29.9 had a weaker peak at 10 nm. Furthermore, when the lignin removal level was lower than 29.9%, the peak at 3 nm remains, suggesting that the PMMA distribution efficiency in smaller 3-nm mesopores was greatly lower than in the larger 10-nm mesopores. As lignin removal increased, the 3-nm peak almost disappeared.

The above results revealed that when the lignin removal was lower than 29.9%, the PMMA distribution efficiency in smaller mesopores was greatly lower than that in larger mesopores. Here were the pores of 3 nm and 10 nm, respectively, when the lignin removal exceeded 29.9%, the PMMA distribution efficiency in the two mesopores showed the opposite pattern. After PMMA occupied the cell wall, the number of mesopores in DW within 29.9–51.7% lignin removal was reduced. When lignin removal reached 97.3%, all the mesopores detected in this study disappeared. In combination with Table 3, it could be seen that delignification promoted the distribution of PMMA in the wood cell wall pores. When the lignin was almost completely cleared away, all the mesopores in the cell walls were charged with PMMA. The natural pores enlarged to the diameter of 3–4 nm mixed in the cellulose microfibrils due to the removal of lignin were unveiled to the non-polar monomers. After being impregnated with polymer, not only commonly known cell cavities but also cell wall pores were refilled. The results confirmed that PMMA was distributed in the transparent wood cell wall on the nanoscale using the small-angle neutron diffraction technique in the case of large lignin removal by Chen

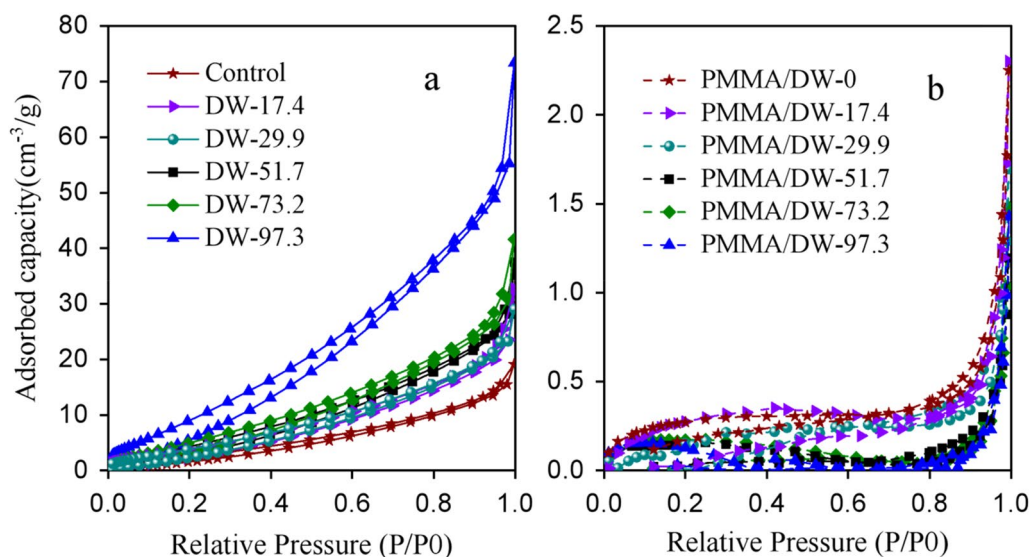


**Fig. 5** Nitrogen adsorption–desorption isotherms of DW (a) and PMMA/DW (b)

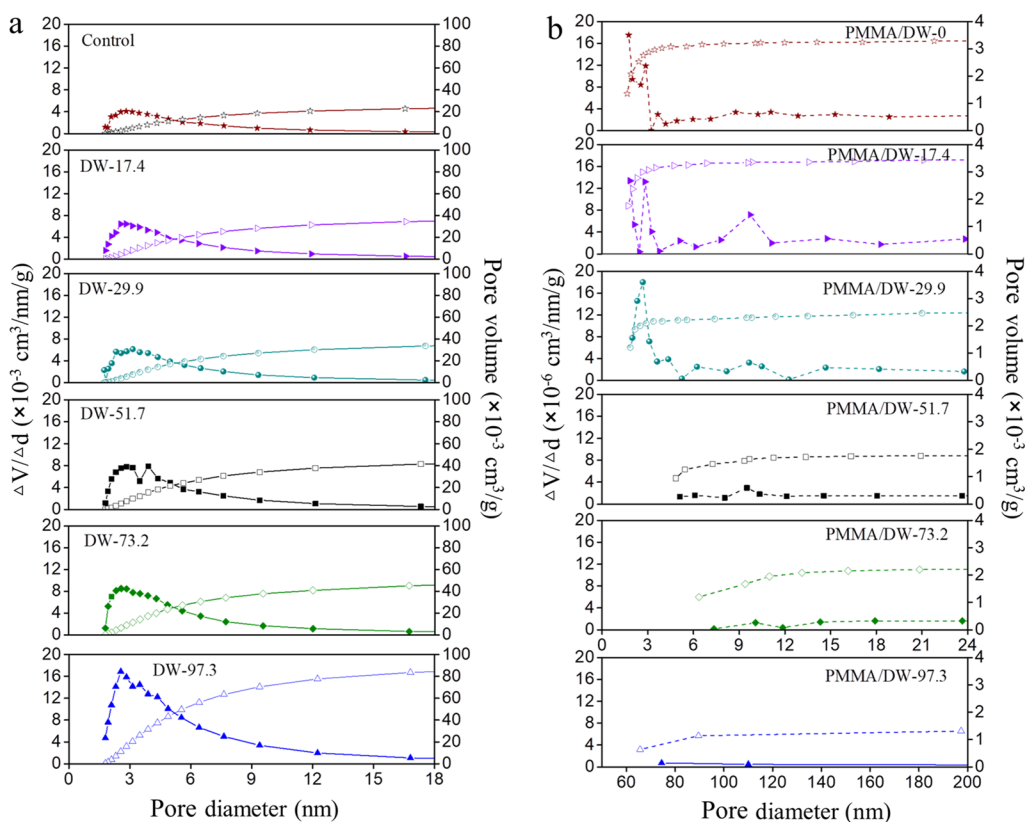


**Fig. 6** Mesopore-size distribution and accumulated volume of DW (a) and PMMA/DW (b). The horizontal axis range of control and DW-17.4,29.9,51.7,73.2,97.3 are 0–18. The horizontal axis range of PMMA / DW-0,17.4,29.9,51.7,73.2 are 0–24, and the horizontal axis range of PMMA / DW-97.3 is 60–200

**Table 2** Specific surface area ( $S_{BET}$ ) and total pore volume ( $V_{total}$ ) of the delignified wood (DW)

Samples	$S_{BET}$ (m <sup>2</sup> /g)	$V_{total}$ ( $\times 10^{-3}$ cm <sup>3</sup> /g)
Control	15.1298	27.1
DW-17.4	23.6308	40.1
DW-29.9	27.0282	41.2
DW-51.7	31.8868	47.8
DW-73.2	36.2904	54.3
DW-97.3	71.3155	94.8

**Table 3** Specific surface area ( $S_{BET}$ ) and total pore volume ( $V_{total}$ ) of the polymethyl methacrylate/delignified wood (PMMA/DW)

Samples	$S_{BET}$ (m <sup>2</sup> /g)	$V_{total}$ ( $\times 10^{-3}$ cm <sup>3</sup> /g)
PMMA/DW-0	0.9975	3.482
PMMA/DW-17.4	1.1676	3.560
PMMA/DW-29.9	1.4671	2.623
PMMA/DW-51.7	0.5046	1.848
PMMA/DW-73.2	0.5848	2.288
PMMA/DW-97.3	0.2946	1.526

et al. [33]. But under the situation of insufficient lignin removal work, the non-polar monomer plastic polymer can hardly enter the common target cell walls.

**Dimensional stability**

To explore the influence of PMMA impregnation on the dimensional stability of DW, the volume-swelling coefficient and anti-swelling efficiency of the samples were also analyzed here. As shown in Fig. 7a, the results showed

that the  $\alpha_{65\%}$  and  $\alpha_{max}$  of PMMA/DW-0 were significantly reduced compared to the natural wood. Corresponded  $ASE_{65\%}$  and  $ASE_{max}$  of the PMMA/DW-0 reached 29.34% and 37.03%, respectively. Figure 7b shows that the combination of PMMA and wood effectively reduced the moisture absorption and water absorption of wood. However, the  $\alpha_{65\%}$  and  $\alpha_{max}$  of the PMMA/DW began to increase with the delignified process. The  $ASE_{65\%}$  and  $ASE_{max}$  of PMMA/DW-17.4 were significantly reduced, which



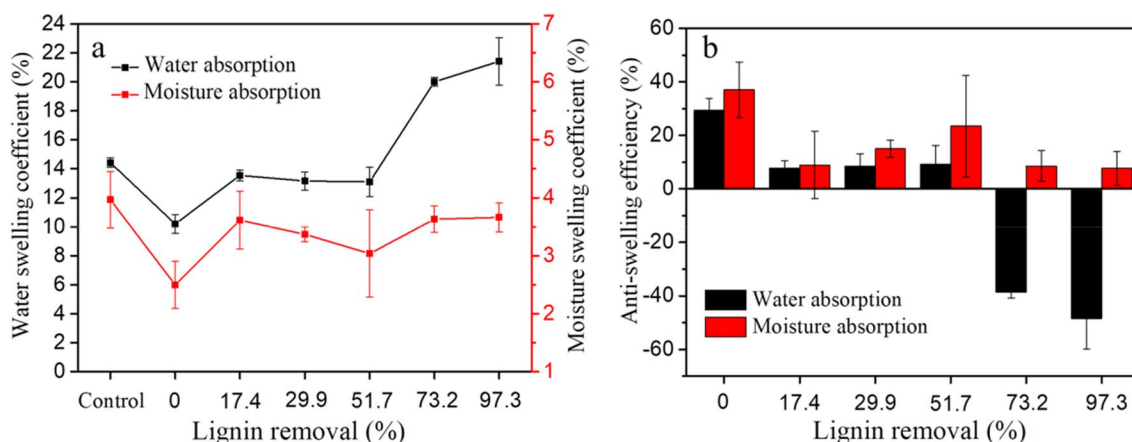


**Fig. 7** The swelling coefficient of water and moisture absorption of natural wood and PMMA/DW (a) and the volumetric anti-swelling efficiency of moisture and water absorption of PMMA/DW (b)

was due to the partial removal of lignin causing the cell wall to expose more hydrophilic hydroxyl groups to the water [43]. Interestingly,  $\alpha_{65\%}$  and  $\alpha_{max}$  of PMMA/DW decreased when the lignin removal reached 29.9%. This phenomenon can be assumed to be because when the lignin removal exceeds 29.9%, the resin begins to penetrate the cell wall and polymerize in situ to generate PMMA. The absorption of water by the hydroxyl group was hindered molecularly due to the distribution and occupation of PMMA in the nanopores of the cell wall, thereby inhibiting the change in the cell wall size. Furthermore, the  $\alpha_{65\%}$  and  $\alpha_{max}$  of PMMA/DW continued to decrease and the corresponding  $ASE_{65\%}$  continued to improve thereafter. This was owing to more polymer joining the cell wall and filling the nanostructure pores. This was consistent with the above result of pore-size distribution showing the number of 10 nm pores in PMMA/DW

decreased when the lignin removal reached 29.9%. When the lignin removal reached 51.7%, the mesopores with a diameter of about 3 nm disappeared. This phenomenon may be due to the further penetration of plastics and the filling of nanopores in the cell wall. This also explained why the  $ASE_{65\%}$  and  $ASE_{max}$  of PMMA/DW-51.7 continued to increase. However,  $\alpha_{65\%}$  and  $\alpha_{max}$  of PMMA/DW were successively increased as the lignin removal continued to increase. Correspondingly,  $ASE_{65\%}$  also decreased obviously and  $ASE_{max}$  even had a negative value. This was probably attributable to the increasing proportion of PMMA in the composite system as the degree of chemical treatment enhanced and the original strong chemical bond in the composite system was replaced just by more physical filling. This might exacerbate the interface separation between cellulose and PMMA and ultimately led to poor dimensional stability.

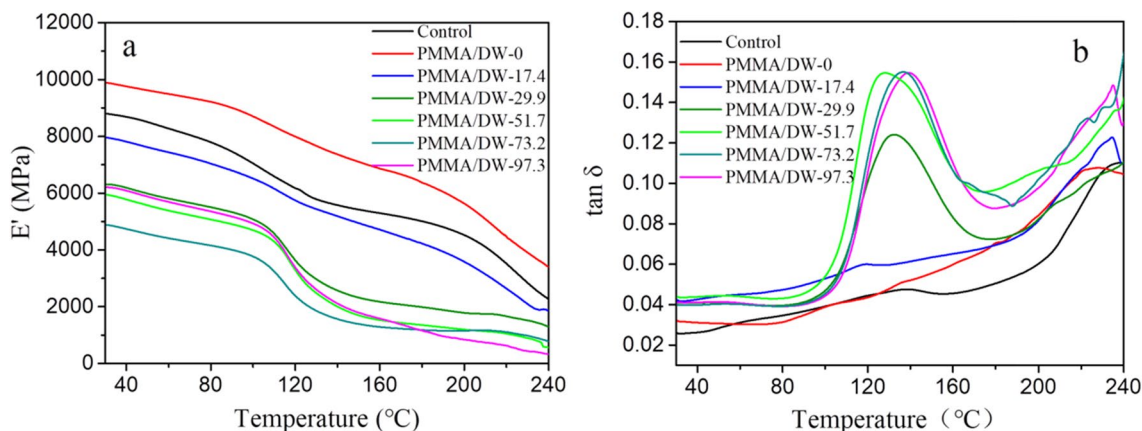


**Fig. 8** Dynamic mechanical properties of PMMA/DW. Storage modulus ( $E'$ ) of natural wood and PMMA/DW (a). Loss tangent ( $\tan \delta$ ) of control and PMMA/DW (b)

### Dynamic mechanical properties

As shown in Fig. 8a, the storage modulus  $E'$  of the natural wood and PMMA/DW decreased with the increase in temperature owing to the increase in the fluidity of the high molecular polymer in the wood. The  $E'$  of the original wood decreased significantly at about 220 °C. The flexibility increase of the amorphous part of wood undertook relevant local responsibilities. The appearance of this phenomenon was mainly caused by the micro-Brownian motion of the molecular chains of the cellulose amorphous region [23]. The  $E'$  of PMMA/DW-0 at room temperature increased to 9887 MPa from 8798 MPa of the original wood, which showed that the PMMA filling only in the cell lumen could effectively improve the elasticity of wood. However, the  $E'$  of PMMA/DW gradually decreased when the lignin removal rose. As a filling matrix for the cell wall, lignin can fix the cellulose molecular chains and hinder their free movement. When the lignin content of the cell wall was reduced, it was easier for the slippage to occur among the cellulose macromolecule chains, which directly caused the rigidity of the wood to drop. However, PMMA only filled DW in a separate form, which did little to improve the stiffness of the composite. The  $E'$  of PMMA/DW-97.3 increased when the lignin removal reached 97.3%. This was owing to the plastic fully penetrating the cell wall, more nanoscale pores being filled and the molecular weight of PMMA gradually increasing, thereby the rigidity was improved.

Figure 8b shows the relationship between the loss tangent ( $\tan\delta$ ) of the wood and temperature. The  $\tan\delta$  of the natural wood and PMMA/DW increased with the temperature raising. This was because the viscosity of the polymer in the wood increased with the heightening of temperature and the transition from elasticity to viscosity was a typical feature of wood viscoelasticity [44]. When the lignin removal reached 29.9%, the  $\tan\delta$  increased significantly at 130 °C which was the glass transition temperature corresponding to PMMA [45]. When the lignin removal surpassed 51.7%, the  $\tan\delta$  remained at the maximum level. It meant that the proportion of PMMA in the PMMA/DW system further increased as the lignin removal rose. Besides, the  $\tan\delta$  of PMMA/DW increased overall as the lignin removal level improved. This was owing to more pores being created in the cell wall as the lignin was removed, which facilitated the penetration and aggregation of plastic in the cell wall and replaced the original lignin. The combination method of cell wall components changed from the original chemical combination between cellulose and lignin to the current physical combination between cellulose and PMMA. The degree of cross-linking between the cellulose molecular chains was further reduced, so there would be more energy loss

when the molecular chains moved. This leads the  $\tan\delta$  of PMMA/DW to improve more.

### Micromechanical properties

Micromechanical properties of the natural wood and PMMA/DW cell walls were investigated by nanoindentation. Hardness, indentation modulus, and typical indentation load–depth curves of the cell wall are presented in Fig. 9, respectively. Compared with the original wood, the hardness and indentation modulus of PMMA/DW-0 were unchanged (Fig. 9d, e). This indicated that PMMA only loaded in the cell lumen and had not yet been seeded in the cell wall. The hardness and indentation modulus of PMMA/DW-17.4 were reduced by 22.92% and 6.14% compared with PMMA/DW-0, respectively. When the lignin removal got 29.9%, the hardness and indentation modulus of PMMA/DW-29.9 began to increase. Since then, the hardness and indentation modulus of PMMA/DW also improved as the delignification process was promoted. After almost all lignin had been taken away, the hardness and indentation modulus of PMMA/DW-97.3 increased by 38.54% and 81.76% compared with PMMA/DW-0, respectively. The above results indicated that when the degree of delignification was light, the hardness and indentation modulus of the cell wall tended to go down because partial lignin was removed and the polymer had not moved into the cell wall by the common processing conditions. When the lignin removal exceeded 29.9%, the Nanoindentation tested hardness and indentation modulus of the cell wall increased significantly ( $P < 0.05$ ). This owed to the Nano field porosity of the wood cell wall increased as the lignin was further removed and made the polymer combined with the cell wall in the nanoscale. This promoted the penetration of MMA in the cell wall. After that, more MMA resided and polymerized in the cell wall Nano voids which gifted the cell wall more excellent mechanical properties.

### Conclusions

Based on the poor permeability of non-polar monomers such as MMA in the delignification template, may cause the bad dimensional stability and mechanical properties of wood-based functional materials. In this paper, MMA was used to impregnate the wood with different lignin removal ratios; and then polymerized in situ to obtain PMMA/DW. The WPG results showed that the removal of lignin was beneficial to increase the weight of PMMA/DW, and the density of PMMA/DW also improved. When the lignin removal reached 97.3%, the density of PMMA/DW-97.3 was 1.15 g/cm<sup>3</sup>, which was the same density as pure PMMA. The results of nitrogen adsorption showed that the number and diameter of mesopores

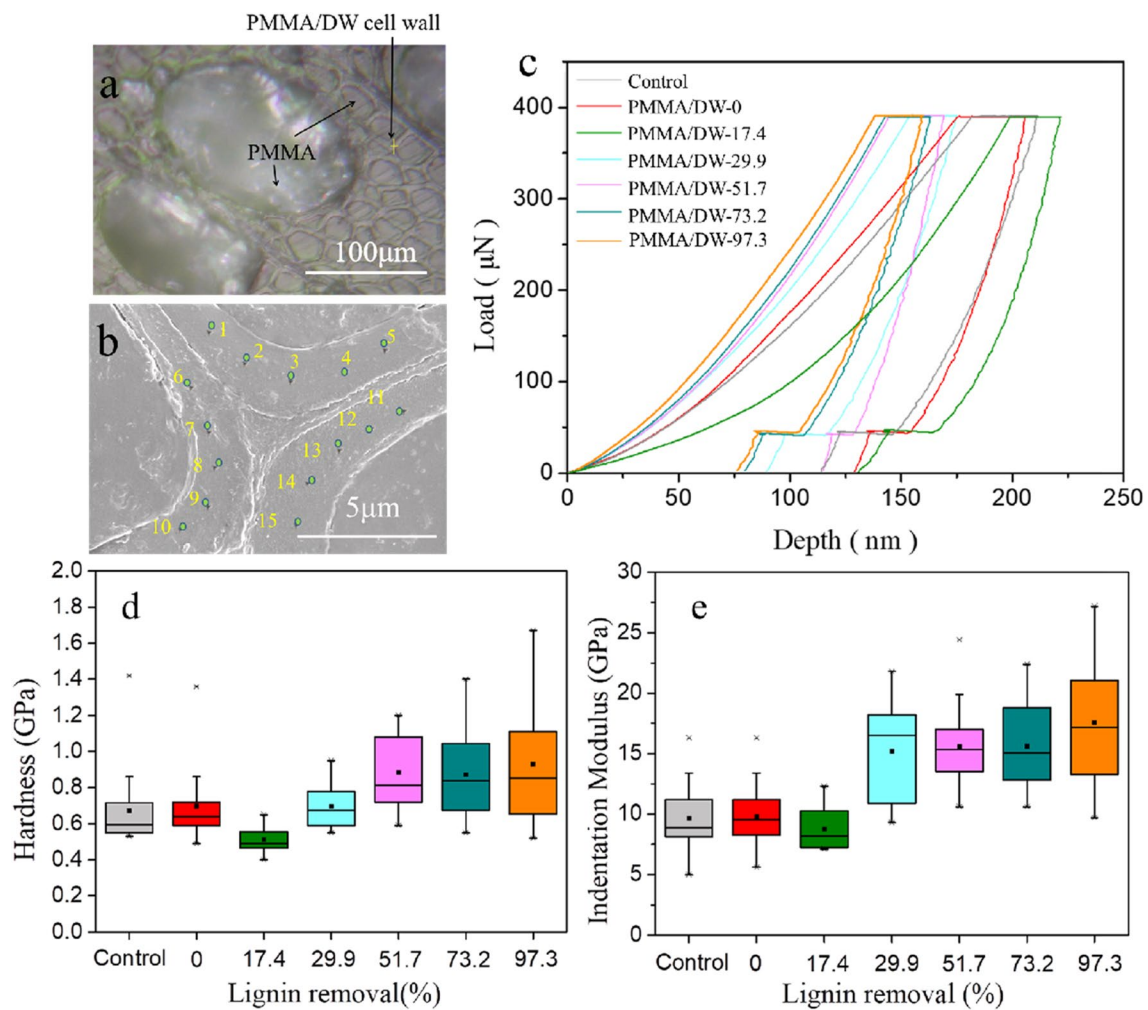


**Fig. 9** Micromechanical properties of PMMA/DW. Optical micrograph of the transverse section of PMMA/DW (a). FE-SEM image of wood cell walls after nanoindentation (b). Fifteen effective points were selected for each sample to calculate the average value. Typical indentation load–depth curves of cell wall (c). Hardness of PMMA/DW cell wall (d). Indentation modulus of PMMA/DW cell wall (e)

with 3 nm pore size of wood increased with the raise of lignin removal. When the lignin removal reached 29.9%, the number of mesopores with a 10 nm pore diameter of PMMA/DW-29.9 gradually reduced, indicating that resin penetrated the cell wall in this diameter range. When the lignin removal reached 51.7%, all mesopores with a pore size of 3 nm of PMMA/DW-51.7 disappeared, revealing that plastic was distributed in smaller mesopores in the cell wall. The reduction of PMMA/DW-29.9 of the larger mesopores and the disappearance of PMMA/DW-51.7 of the smaller mesopores further indicate that the removal of lignin is beneficial to the penetration of polymer in the wood cell wall. The subsequent increase in  $ASE_{65\%}$  and  $ASE_{max}$  of PMMA/DW-29.9 and PMMA/DW-51.7 confirmed that the filling of plastic on the cell wall nanopores

improved the dimensional stability of wood. DMA results showed that the storage modulus of PMMA/DW generally decreased with the exchange of PMMA and lignin in wood, which was caused by the poor combination of non-polar monomer polymer and wood polar components. The nanoindentation results show that when the lignin removal reached 29.9%, the indentation modulus and hardness of the PMMA/DW cell wall significantly increased, which indicated that plastic was uniformly dispersed in the cell wall and the mechanical properties of the cell wall were remarkably improved. The significant enhancement of the cell wall mechanical properties at a lignin removal of 29.9% determined that the delignification level regarding the occupation of non-polar resin in the wood cell wall was 29.9%. This study takes MMA as

the research object to provide data for the dispersibility of non-polar monomers in delignified wood, as well as a reference for the dimensional stability and mechanical properties of such polymer/wood-based functional materials.

#### Abbreviations

MMA	Methyl methacrylate
DW	Delignified wood
PMMA/DW	Polymethyl methacrylate/delignified wood
WPG	Weight percent gain
FE-SEM	Field emission scanning electron microscope
ATR-FTIR	Attenuated total reflection Fourier infrared spectroscopy
BET	Brunauer–Emmett–Teller
$S_{BET}$	Specific surface area
BJH	Barrett–Joyner–Halenda
$\alpha_{65\%}$	Volume swelling coefficient of moisture absorption
$\alpha_{max}$	Volume swelling coefficient of water absorption
$ASE_{65\%}$	Volumetric anti-swelling efficiency of moisture absorption
$ASE_{max}$	Volumetric anti-swelling efficiency of water absorption
DMA	Dynamic mechanical analysis
$E'$	Storage modulus
$\tan \delta$	Loss tangent

#### Acknowledgements

Thanks to “the Advanced analysis and testing center of Nanjing Forestry University” for the professional and thoughtful testing services.

#### Author contributions

HZ: conceptualization, methodology, resources, writing—original draft, project administration. FX: data curation, writing—original draft, formal analysis, investigation, visualization. LX: methodology, writing—original draft. CZ: formal analysis, investigation. All authors read and approved the final manuscript.

#### Funding

This work was financially supported by the National Natural Science Foundation of China (31870543) and the Youth Science and Technology Innovation Fund of Nanjing Forestry University (cx2016017).

#### Availability of data and materials

All data discussed during this study are included in this published article.

#### Declarations

#### Competing interests

The authors declare that they have no competing interests.

Received: 23 May 2022 Accepted: 8 February 2023

Published online: 22 February 2023

#### References

- Ling S, Kaplan DL, Buehler MJ (2018) Nanofibrils in nature and materials engineering. *Nat Rev Mater* 3:18016. <https://doi.org/10.1038/natrevmats.2018.16>
- Zhu H, Luo W, Ciesielski PN, Fang Z (2016) Wood-derived materials for green electronics, biological devices, and energy applications. *Chem Rev* 116:9305–9374. <https://doi.org/10.1021/acs.chemrev.6b00225>
- Fahlén J, Salmén L (2003) Cross-sectional structure of the secondary wall of wood fibers as affected by processing. *J Mater Sci* 38:119–126. <https://doi.org/10.1023/A:1021174118468>
- Berglund LA (2018) Bioinspired wood nanotechnology for functional materials. *Adv Mater* 30:1704285. <https://doi.org/10.1002/adma.201704285>
- Chen C, Kuang Y, Zhu S, Burgert I, Hu L (2020) Structure–property–function relationships of natural and engineered wood. *Nat Rev Mater* 5:1–25. <https://doi.org/10.1038/s41578-020-0195-z>
- Keplinger T, Cabane E, Chanana M, Hass P, Burgert I (2015) A versatile strategy for grafting polymers to wood cell walls. *Acta Biomater* 11:256–263. <https://doi.org/10.1016/j.actbio.2014.09.016>
- Fu Q, Ansari F, Zhou Q, Berglund L (2018) Wood nanotechnology for strong, mesoporous, and hydrophobic biocomposites for selective separation of oil/water mixtures. *ACS Nano* 12:2222–2230. <https://doi.org/10.1021/acs.nano.8b00005>
- Schwarzkopf M (2020) Densified wood impregnated with phenol resin for reduced set-recovery. *Wood Mater Sci Eng* 16:1–7. <https://doi.org/10.1080/17480272.2020.1729236>
- Zhu M, Song J, Li T, Gong A (2016) Highly anisotropic, highly transparent wood composites. *Adv Mater* 28:5181–5187. <https://doi.org/10.1002/adma.201600427>
- Li Y, Fu Q, Yu S, Yan M, Berglund L (2016) Optically transparent wood from a nanoporous cellulosic template: combining functional and structural performance. *Biomacromol* 17:1358–1364. <https://doi.org/10.1021/acs.biomac.6b00145>
- Mi R, Chen C, Keplinger T, Pei Y, Hu L (2020) Scalable aesthetic transparent wood for energy efficient buildings. *Nat Commun* 11:3836. <https://doi.org/10.1038/s41467-020-17513-w>
- Li T, Zhang X, Lacey SD, Mi R, Zhao X, Jiang F (2019) Cellulose ionic conductors with high differential thermal voltage for low-grade heat harvesting. *Nat Mater* 18:608–613. <https://doi.org/10.1038/s41563-019-0315-6>
- Wu M, Huang S, Liu C, Wu J, Agarwal S, Greiner A (2020) Carboxylated wood-based sponges with under oil superhydrophilicity for deep dehydration of crude oil. *J Mater Chem A* 8:11354–11361. <https://doi.org/10.1039/D0TA03844J>
- Gabrieli I, Gatenholm P, Glasser WG, Jain RK (2000) Separation, characterization and hydrogel-formation of hemicellulose from aspen wood. *Carbohydr Polym* 43:367–374. [https://doi.org/10.1016/S0144-8617\(00\)00181-8](https://doi.org/10.1016/S0144-8617(00)00181-8)
- Gabrieli I, Gatenholm P (1998) Preparation and properties of hydrogels based on hemicellulose. *J Appl Polym Sci* 69:1661–1667. [https://doi.org/10.1002/\(SICI\)1097-4628\(19980822\)69:8%3c1661::AID-APP19%3e3.0.CO;2-X](https://doi.org/10.1002/(SICI)1097-4628(19980822)69:8%3c1661::AID-APP19%3e3.0.CO;2-X)
- Nie KC, Wang Z, Tang R, Zheng L, Li C, Shen X (2020) Anisotropic, flexible wood hydrogels and wrinkled, electrodeposited film electrodes for highly sensitive, wide-range pressure sensing. *ACS Appl Mater Inter* 12:43024–43031. <https://doi.org/10.1021/acsami.0c13962>
- Li J, Lu Y, Yang D, Sun Q, Liu Y, Zhao H (2011) Lignocellulose aerogel from wood-ionic liquid solution (1-allyl-3-methylimidazolium chloride) under freezing and thawing conditions. *Biomacromol* 12:1860–1867. <https://doi.org/10.1021/bm200205z>
- Yang S, Yu J, Tang X, Ge J, Ding B (2014) Ultralight nanofibre-assembled cellular aerogels with superelasticity and multifunctionality. *Nat Commun* 5:5802. <https://doi.org/10.1038/ncomms6802>
- Song J, Chen C, Yang Z, Kuang YD, Li T, Li Y (2017) Highly compressible, anisotropic aerogel with aligned cellulose nanofibers. *ACS Nano* 12:140–147. <https://doi.org/10.1021/acs.nano.7b04246>
- Fu Q, Chen Y, Sorieul M (2020) Wood-based flexible electronics. *ACS NANO* 14:3528–3538. <https://doi.org/10.1021/acs.nano.9b09817>
- Liu Y, Zhou J, Chen L, Zhang P (2015) Highly flexible freestanding porous carbon nanofibers for electrodes materials of high-performance all-carbon supercapacitors. *ACS Appl Mater Inter* 7:23515–23520. <https://doi.org/10.1021/acsami.5b06107>
- Wang Z, Luo Y, Wu K, Liu T (2019) Fabrication and characterization of thermal-responsive biomimetic small-scale shape memory wood composites with high tensile strength, high anisotropy. *Polymers-Basel* 11:1892. <https://doi.org/10.3390/polym11111892>
- Zhu Z, Zhu Y (2015) Preparation and Properties of Porous Composite of Hematite/Magnetite/Carbon with Eucalyptus Wood Biotemplate. *Mater Manuf Process* 30:285–291. <https://doi.org/10.1080/10426914.2014.941478>
- Beg M, Picker K (2006) Fiber Pretreatment and Its Effects on Wood Fiber Reinforced Polypropylene Composites. *Mater Manuf Process* 21:303–307. <https://doi.org/10.1080/10426910500464750>
- Li T, Song J, Zhao X, Yang Z, Pastel G, Xu S. Anisotropic, lightweight, strong, and super thermally insulating nanowood with naturally aligned

- nanocellulose. *Sci Adv* 2018;4:eaau3724. <https://doi.org/10.1126/sciadv.aar3724>.
26. Li T, Li S, Kong W, Chen C, Hitz E, Jia C. (2019) A nanofluidic ion regulation membrane with aligned cellulose nanofibers. *Sci Adv* 5:eaau4238. <https://doi.org/10.1126/sciadv.aau4238>.
  27. Jiang F, Li T, Li Y, Zhang Y (2018) Wood-based nanotechnologies toward sustainability. *Adv Mater* 30:1703453. <https://doi.org/10.1002/adma.201703453>
  28. Klein KC, Krause A, Pilz SE, Brischke C (2020) High-energy multiple impact (HEMI) tests of wood–polypropylene composites: new insights in structural integrity. *Wood Mater Sci Eng* 16:1–4. <https://doi.org/10.1080/17480272.2020.1737962>
  29. Xu F, Zhang H, Wu J (2021) Synergistic catalytic flame retardant effect of zirconium phosphate on the poplar plywood. *Constr Build Mater* 290:123208. <https://doi.org/10.1016/j.conbuildmat.2021.123208>
  30. Schaefer DW, Justice RS (2010) How nano are nanocomposites? *Macromolecules* 40:8501–8517. <https://doi.org/10.1021/ma070356w>
  31. Guo J, Chen J, Li R, Liu J, Luo R, Jiao L, Yin Y (2022) Thermoporometry of waterlogged archaeological wood: Insights into the change of pore traits after the water-removal by supercritical drying. *Themocimica Acta* 715:179297. <https://doi.org/10.1016/j.tca.2022.179297>
  32. Schneider MH, Brebner KI, Hartley ID (1991) Swelling of a cell lumen filled and a cell-wall bulked wood polymer composite in water. *Wood Fiber Sci J Soc Wood Sci Technol* 23:165–172. <https://doi.org/10.1177/004051759106100410>
  33. Chen P, Li Y, Nishiyama Y, Pingali SV, Berglund LA (2021) Small angle neutron scattering shows nanoscale pmma distribution in transparent wood biocomposites. *Nano Lett* 21:2883–2890. <https://doi.org/10.1021/acs.nanolett.0c05038>
  34. Agarwal UP (2006) Raman imaging to investigate ultrastructure and composition of plant cell walls: distribution of lignin and cellulose in black spruce wood (*Picea mariana*). *Planta* 224:1141–1153. <https://doi.org/10.1007/s00425-006-0295-z>
  35. Tze WTY, Wang S, Rials TG, Pharr GM, Kelly SS (2007) Nanoindentation of wood cell walls: continuous stiffness and hardness measurements. *Compos Part A-Appl S* 38:945–953. <https://doi.org/10.1016/j.compositesa.2006.06.018>
  36. Wang J, Deng Y, Yon Q, Qiu X, Yuan R, Yang D (2016) Reduction of lignin color via one-step UV irradiation. *Green Chem* 18:695–699. <https://doi.org/10.1039/c5gc02180d>
  37. Morii H, Nakamiya K, Kinoshita S (1995) Isolation of a lignin-decolorizing bacterium. *Bioengineering* 80:296–299. [https://doi.org/10.1016/0922-338X\(95\)90835-N](https://doi.org/10.1016/0922-338X(95)90835-N)
  38. Kafle K, Shi R, Lee CM, Mittal A, Park YB, Sun Y (2014) Vibrational sum-frequency-generation (SFG) spectroscopy study of the structural assembly of cellulose microfibrils in reaction woods. *Cellulose* 21:2219–2231. <https://doi.org/10.1007/s10570-014-0322-3>
  39. Bandounas L, Wiercx NJ, Winde J, Ruijsenaars HJ (2011) Isolation and characterization of novel bacterial strains exhibiting ligninolytic potential. *Bmc Biotechnol* 11:94. <https://doi.org/10.1186/1472-6750-11-94>
  40. Atalla RH, Agarwal UP (1985) Raman microprobe evidence for lignin orientation in the cell walls of native woody tissue. *Science* 227:636–638. <https://doi.org/10.1126/science.227.4687.636>
  41. Cheng SK, Chen C (2004) Mechanical properties and strain-rate effect of EVA/PMMA in situ polymerization blends. *Eur Polym J* 40:1239–1248. <https://doi.org/10.1016/j.eurpolymj.2003.11.022>
  42. Habibi Y, Lucia LA, Rojas OJ (2010) Cellulose nanocrystals: chemistry, self-assembly, and applications. *Chem Rev* 110:3479–3500. <https://doi.org/10.1021/cr900339w>
  43. Yang T, Cao J, Ma E (2019) How does delignification influence the furfurylation of wood? *Ind Crop Prod* 135:91–98. <https://doi.org/10.1016/j.indcrop.2019.04.019>
  44. Hristov V, Vlachopoulos J (2007) A study of viscoelasticity and extrudate distortions of wood polymer composites. *Rheol Acta* 46:773–783. <https://doi.org/10.1007/s00397-007-0186-7>
  45. Roos SG, Müller AHE, Matyjaszewski K (1999) Copolymerization of n-butylacrylate with methyl methacrylate and PMMA macromonomers: Comparison of reactivity ratios in conventional and atom transfer radical polymerization. *Macromolecules* 32:8331. <https://doi.org/10.1017/S0031182000041019>

## Publisher's Note

Springer Nature remains neutral with regard to jurisdictional claims in published maps and institutional affiliations.

Submit your manuscript to a SpringerOpen® journal and benefit from:

- Convenient online submission
- Rigorous peer review
- Open access: articles freely available online
- High visibility within the field
- Retaining the copyright to your article

---

Submit your next manuscript at ► [springeropen.com](https://www.springeropen.com)

---